Joint effects of differential diffusion and the stratification length-scale on flame kernel development

A. Er-raiy *, R. Boukharfane †, and M. Parsani ‡
King Abdullah University of Science and Technology (KAUST),
Computer Electrical and Mathematical Science and Engineering Division (CEMSE),
Extreme Computing Research Center (ECRC), 23955-6900, Thuwal, Saudi Arabia

Early flame kernel development and propagation in globally lean stratified fuel–air mixtures is of importance in various practical devices such as internal combustion engines. In this work, three-dimensional direct numerical simulation (DNS) is used to study the influence of the differential diffusion effects in a globally lean methane–air mixtures in presence of mixture heterogeneities with the goal of understanding the flame kernel behavior in such conditions. The DNS typical configuration corresponds to a homogeneous isotropic flow with an expanding spherical flame kernel. The local forced ignition of the kernel is performed by appending as source term in the sensible enthalpy transport equation that emulates spark ignition by energy deposit for a prescribed duration. The combustion chemistry is described with a skeletal methane-air mechanism, which i) features 14 species and 38 reactions, and ii) uses a multicomponent approach to evaluate transport coefficients. To assess the joint effects of differential diffusion and the stratification characteristic length-scale L_Φ on the flame kernel development, we considered cases with constant (unitary) and variable fuel Lewis number, both with different values for L_Φ.

I. Introduction

In a wide range of practical devices, the early combustion stage that follows the ignition plays a key role in ensuring proper and efficient functioning. For example, in the spark ignition engines, this stage

*Postdoctoral research fellow, aimad.erraiy@kaust.edu.sa, AIAA member
†Postdoctoral research fellow, radouan.boukharfane@kaust.edu.sa, AIAA member
‡Assistant Professor, matteo.parsani@kaust.edu.sa, AIAA Member

significantly influences the combustion stability, which in turn could impact the overall engine performance in terms of efficiency and pollutant emissions. Indeed, during the combustion process in such engines, the early flame kernel development stage is shown to be one of the leading causes of the occurrence of cycle-to-cycle variations [1].

Moreover, in most engineering application, the forced ignition and the development of the flame kernel do not occur in a perfectly homogeneous fuel-oxidizer mixtures [2], *i.e.*, the chemical reactions mainly occur in a mixture where the equivalence ratio distribution is heterogeneous or stratified. Indeed, stratified premixed combustion has proven to be an efficient approach to extend the flammability limits, improve combustion stability and lower pollutant formation.

To better understand the dynamics and parameters that influence the propagation of a flame kernel in a stratified mixture, a number of previous works [3, 4] has shown that, along with other factors, the the differential diffusion of heat and mass has a considerable influence on the localized forced ignition. The differential diffusion is often quantified by the non-dimensional ratio of the fuel thermal and mass diffusivities, *i.e* , $Le_F = \lambda_F / D_F$. Evidences of the effects of differential diffusion have been widely studied experimentally in the framework of spherical flame expansion [5–7]. However, numerical studies have been considered to complete these studies due to the inaccessibility to the finest structures statistics from experimental measurements and make it possible to draw more general conclusions.

Previous homogeneous flame kernel development DNS analyses showed that differential diffusion tends to increase the flame speed and accelerate the overall flame expansion [8]. Furthermore, flame curvature dynamics was shown to be sensitive to Lewis number [9], in particular at low pressures [10]. On the other hand, flame kernel ignition dynamics have been shown to be strongly influenced by the fuel Lewis number, even in inhomogeneous mixtures [11]. In particular, using a single-step chemistry, [11] systematically varied the characteristics of the fresh gases mixtures such as the Taylor-micro scale L_Φ and the variance of the stratified mixture fraction field and considered a set of three Lewis numbers ranging from 0.8 to 1.2. One of the major conclusions drawn by [11] is the fact that the flame kernel burning extent and combustion self-sustainability are highly dependent on the fuel Lewis number and on the characteristic scale L_Φ and that the extent of burning is non-monotonic as a function of these parameters.

The present work aims at completing the DNS previous studies that were mainly performed using a single-step chemistry. Indeed, considering a detailed chemistry will be of interest to investigate the role of differential diffusion in the development and the propagation of a flame kernel in a stratified mixture. In this study, of a new set of DNS simulations is generated to perform a parametric study featuring the stratification length scale L_Φ with a 14 species methane-air mechanism. Furthermore, the differential diffusion effects are addressed as the DNS database considers both constant and variable fuel Lewis numbers. The present paper is organized as follows. The governing equations, numerical methods and the initialization methodology relevant to the current study are first presented. Subsequently, the results are discussed. Finally, the main conclusions and future works will be drawn in the final section of the paper.

II. Numerical methods and simulation details

A. Governing equations

In this work, the low Mach number (LMN) approximation of the fully compressible Navier–Stokes equations (NSE) is considered. Thanks to the LMN approximation, the compressible NSE can be simplified such that the thermo-chemical state of the flow is decoupled from the momentum equation [12]. In this framework, the mass conservation equation is expressed as

$$\partial_t \rho + \nabla \cdot (\rho \mathbf{u}) = 0, \tag{1}$$

where ρ and $\mathbf{u}$ are respectively the mixture density and the velocity vector. The pressure is split in two components: (i) a space-uniform thermodynamic pressure, $P^{(0)}(t)$, and a hydrodynamic pressure, $P^{(1)}(\boldsymbol{x}, t)$, linked to the fluid motion. Hence, the momentum conservation equation reads

$$\partial_t \rho \mathbf{u} + \nabla \cdot (\rho \mathbf{u}\mathbf{u}) = -\nabla P^{(1)} + \nabla \cdot \tau, \tag{2}$$

with τ the viscous stress tensor, which takes the following form for a Newtonian fluid

$$\tau = \mu \left(\nabla \mathbf{u} + \nabla \mathbf{u}^T \right) - \frac{2}{3} \mu \left(\nabla \cdot \mathbf{u} \right) \mathbf{I}, \tag{3}$$

where μ and $\mathbf{I}$ are the mixture dynamic viscosity and the identity tensor, respectively. In addition to momentum and density, the primary transported variables are the species mass fractions, Y_k, and the sensible enthalpy, h_s, expressed as

$$h_s = \sum_{k=1}^{\mathcal{N}_{\text{sp}}} Y_k h_{s,k}, \tag{4}$$

where $h_{s,k}$ denotes the sensible enthalpy of the kth species. For each species k the transport equation of Y_k is written

$$\partial_t \rho Y_k + \nabla \cdot (\rho \mathbf{u} Y_k) = \nabla \cdot (\rho \mathcal{D}_k \nabla Y_k) + \dot{\omega}_k, \tag{5}$$

where $\mathcal{D}_k$ is the molecular diffusion coefficient of species k and $\dot{\omega}_k$ is the production/destruction rate of chemical species k. The energy equation requires the greatest attention because multiple form exists. The equation involving sensible enthalpy is preferred [13] and it reads

$$\partial_t \rho h_s + \nabla \cdot (\rho \mathbf{u} h_s) = \frac{\gamma - 1}{\gamma} \frac{D P^{(0)}}{D t} + \dot{\omega}_{h_s} + \nabla \cdot (\lambda \nabla T) - \nabla \cdot \left(\rho \sum_{k=1}^{\mathcal{N}_{\text{sp}}} h_{s,k} Y_k \mathcal{V}_k \right). \tag{6}$$

In the above equation, γ is the ratio of the specific heats, λ is the thermal conductivity, and $\dot{\omega}_{h_s}$ is the resulting heat release rate. This rate is expressed in terms of the species production rates, $\dot{\omega}_k$, and the standard enthalpies of formation $\Delta h^0_{f,k}$ as

$$\dot{\omega}_{h_s} = - \sum_{k=1}^{\mathcal{N}_{\text{sp}}} \dot{\omega}_k \Delta h^0_{f,k}. \tag{7}$$

The quantity $\mathcal{V}_k$ is the corrected molecular diffusion velocity given by

$$\mathcal{V}_k = - \frac{\mathcal{D}_k}{Y_k} \nabla Y_k + \sum_{l=1}^{\mathcal{N}_{\text{sp}}} \mathcal{D}_l \nabla Y_l. \tag{8}$$

The system of equations (1)-(6) is completed by the perfect gas equation of state $P^{(0)} = \rho R T / W$, where the mixture molecular weight W is given by $W = \sum_{k=1}^{\mathcal{N}_{\text{sp}}} W_k / Y_k$, with W_k being the molecular weight of the species k and R the the universal gas constant.

B. Numerical methods

The transport equations of mass, momentum, sensible enthalpy and species mass fractions are solved in dimensionless form on a fully periodic regular Cartesian grid [14]. Transport properties are evaluated with a mixture-averaged transport model whereby the diffusion coefficients for the chemical species are evaluated following [15], whereas the molecular viscosity and thermal conductivity of the mixture are evaluated, respectively, using the formulas of Wilke [16] and Mathur et al. [17]. To assess the influence of differential diffusion on the overall expanding flame behavior, a detailed chemical mechanism is needed. The flame chemistry is represented by a 14 species and 38 reactions [18] and the species sensible enthalpies and specific heat coefficients are obtained using the polynomials provided by Gordon and McBride [19]. The time integration is carried out with a third-order accurate explicit Runge–Kutta scheme with a minimal data storage method, and spatial derivatives are obtained with a fourth order central difference scheme. The advancement in time is based on the fractional step method proposed by Kim and Moin [20] and the subsequent variable-coefficient Poisson equation for pressure differences is solved using a multi-grid method provided by the HYPRE library [21]. The stiff CVODE solver [22] is used to integrate the reaction rates in species transport equations.

C. Typical configuration

The DNS database typical configuration is turbulent expanding spherical flame evolving in a three dimensional periodic box, *i.e* , constant-volume combustion in presence of equivalence ratio fluctuations. The initial isotropic turbulent flow field is generated following the procedure of Rogallo [23] by prescribing the Passot-Pouquet [24] energy spectrum of the velocity fluctuations. In a similar pattern, the same spectral method was used to generate initial turbulent scalar field ζ [25]. The scalar fluctuations are set from a probability density function (PDF) approximated by the β distribution

$$\mathcal{B}(\zeta;\alpha,\beta) = \frac{\zeta^{\alpha-1}(1-\zeta)^{\beta-1}}{\int_0^1 x^{\alpha-1}(1-x)^{\beta-1}dx}, \tag{9}$$

where α and β are given in function of the scalar field mean $\overline{\zeta}$ and variance $\overline{\zeta'^2}$ as

$$\alpha = \overline{\zeta}\left(\overline{\zeta}(1-\overline{\zeta})/\overline{\zeta'^2} - 1\right), \quad \text{and} \quad \beta = \alpha(1-\overline{\zeta})/\overline{\zeta}. \tag{10}$$

The choice of this method was driven by its ability of making possible the generation of bounded scalar fields by prescribing their spatial characteristic lengths L_ζ. Since the initial scalar and velocity are generated independently, special attention was paid to bring consistency between the two fields prior to their use in the flame kernel computation. One reason for this can be, for instance, the fact that the small scales spatial coherency between scalar and velocity fluctuations is vital to reproduce physical turbulence-scalar interactions [26]. An illustration of that would be the potential statistics biasing of the turbulent strains and scalar gradient alignment [27].

To achieve this requirement, a preliminary homogeneous isotropic turbulence computation with the initial generated scalar and velocity fields was conducted for a sufficient time at which the flow reaches a statistically stationary state in terms of turbulent kinetic energy, energy dissipation rate, integral length-scales (for turbulence and scalar) and also the scalar variance.

In order to keep the statistics of the initial fields at the desired values during this simulation, the control-based linear forcing approach of Bassenne et al. [28] was used to achieve statistically steady target values of kinetic energy and energy dissipation rate after several large-eddy turn over times. The method suggested in [28] consists of introducing a source term to the momentum equation, in the form of $\mathcal{A}\mathbf{u}$. The forcing coefficient $\mathcal{A}$ reads

$$\mathcal{A}(t) = \frac{\mathcal{B}}{k(t)}\left(\tau_0\epsilon(t) - \mathcal{G}_1^{-1}\left[k(t) - k_0\right]\right) + \frac{\mathcal{B}-1/2}{\epsilon(t)}\left(\tau_0\mathcal{E}(t) - \mathcal{G}_2^{-1}\left[\epsilon(t) - \epsilon_0\right]\right), \tag{11}$$

with $k(t)$ and $\epsilon(t)$ being the turbulent kinetic energy and the energy dissipation rate, k_0 and ϵ_0 denote their steady mean values respectively and τ_0 is the integral time based on k_0 and ϵ_0 as $(2k_0)/(3\epsilon_0)$. $\mathcal{G}_1$ and $\mathcal{G}_2$ refer to the the controller's time constants set to be less than the Kolmogorov timescale to prevent interference with turbulence energy-containing time scales [28]. The terms $\mathcal{B}$ and $\mathcal{E}$ are expressed in function of the

velocity gradient $\nabla \mathbf{u}$, the Hessians of the velocity vector components $\mathbf{H}(u_i)$ and the molecular viscosity ν as

$$\mathcal{B} = \frac{1}{2}\left(1 + \left[3\tau_0\epsilon(t)/2k(t)\right]^2\right)^{-1},$$
$$\mathcal{E} = -2\nu \,\mathrm{tr}\left\langle \nabla \mathbf{u}^T \, \nabla \mathbf{u} \nabla \mathbf{u} + \nu \sum_{i=1}^{3} \mathbf{H}(u_i)^T \mathbf{H}(u_i)\right\rangle,$$

where the $\langle\cdot\rangle$ refers to the volumetric averaging operator.

Similarly, the scalar field forcing technique of Carroll et al. [29] was adopted to preserve the statistics of the scalar field across all flow scales while reproducing physical turbulent scalar mixing mechanisms. In particular, this technique ensures that, independently of initial conditions, the scalar variance converges to the desired constant value $(\overline{\zeta'^2})_0$. Practically, this technique involves the introduction of an artificial linear source term, *i.e* , $\Gamma\zeta$, to the transport equation of the passive scalar ζ expressed as

$$\Gamma = \tau_R^{-1}\left(\sqrt{(\overline{\zeta'^2})_0/\overline{\zeta'^2}} - 1\right) + \left\langle \chi_\zeta / 2\overline{\zeta'^2}\right\rangle \tag{12}$$

where τ_R^{-1} is a relaxation time scale and $\chi_\zeta \equiv 2D_\zeta \| \nabla \zeta \|$ is the scalar dissipation rate (SDR), D_ζ being the molecular diffusivity. τ_R^{-1} is prescribed in a manner that ensures that the forcing term adjusts smoothly to scalar variance and preventing the introduction of artificial transient behaviors into the scalar field structure. The value retained in this work for this term is in the order of large-eddy turn over time τ_0.

After this preliminary computation, the scalar field is extracted and rescaled to represent the considered range of mixture fractions and used to initialize the composition of fuel and oxidizer species and no forcing is applied during the reactive simulation after the ignition of the flame kernel.

The flame kernel was ignited by adding a source term in the sensible enthalpy transport equation that deposits energy for a prescribed time interval. With a view to simplification, plasma formation, shock wave and other specifics of spark formation are not taken into account in the present study. In a similar fashion to [11, 30–33], the forced localized ignition is accounted for by introducing an additional heat source term in the temperature or the energy transport equation, the ignition term considered herein is modeled following a Gaussian profile as a function of the radius r computed from the center of the domain, *i.e* , $r = \sqrt{\sum_{i=1}^{3}(\mathbf{x} - L/2)}$,

where $\mathbf{x}$ the position of a point in the computational domain and L is the characteristic length of the periodic box. This term is expressed in the following manner:

$$\dot{Q}_{ign}(\mathbf{x},t) = \frac{(\rho h_s)_{ign}(\mathbf{x},t) - \rho h_s(\mathbf{x},t)}{t_{ign}} \exp\left(-\frac{r^2}{2R_{ign}}\right)\Big(H(t) - H(t_{ign})\Big), \tag{13}$$

where R_{ign} denotes the width of the Gaussian distribution, t_{ign} is the ignition duration, $H(t)$ refers to the Heaviside step function, while ρ and h_s denote the density and sensible enthalpy. In the source term definition above the density-sensible enthalpy product $(\rho h_s)_{ign}$ is computed in the zone in which the source term is active as

$$(\rho h_s)_{ign}(\mathbf{x},t) = \rho h_s(T_{ign}, P, Y_k(\mathbf{x},t)) = \frac{P\sum_{k=1}^{N_s} Y_k(\mathbf{x},t) h_{s,k}(T_{ign})}{\mathcal{R}T_{ign}\sum_{k=1}^{N_s} Y_k(\mathbf{x},t)/W_k}, \tag{14}$$

with $Y_k(\mathbf{x},t)$, W_k and $h_{s,k}$ denote respectively the mass fraction, the molecular weight and the sensible enthalpy of the k$^{\text{th}}$ species, N_s the number of the species present in the mixture, P the thermodynamic pressure, $\mathcal{R}$ the gas constant and T_{ign} the prescribed kernel temperature. In order to ensure a successful ignition, the parameters R_{ign}, t_{ign} and T_{ign} should be carefully set to maximize the extent of burning and guarantee the flame self-sustenance.

For instance, the choice of the Gaussian profile width R_{ign} is of great importance as shown in [32–35]. Indeed, the size of the ignition kernel is inextricably linked to the flame self-sustenance and the subsequent thermal expansion. If R_{ign} is too small, the flame extinguishes due to the restricted burning extent. Conversely, if the kernel is relatively large, the simulation may blow-up due the splitting errors arising from the high-intensity thermal expansion. Moreover, even an arbitrary value R_{ign} within the range bounded by these two extreme cases can have detrimental effects on the accuracy of the overall simulation. A good illustration of this would be the poor resolution of the composition gradient or the possibility of inducing artificial transient effects of the forced ignition into the flame structure [34, 35]. In the current DNS database, R_{ign} is set to be in the order of one laminar flame thickness δ_f^0. Such a value was successfully used in the context of localized forced ignition of stratified or homogeneous mixtures [11, 36] with a single-step chemistry. Although our computations are carried out with a skeletal mechanism, the value $R_{ign} \sim 1.1\delta_f^0$ suggested in [11] have

proven to be a robust and reliable choice.

For optimum spark ignition, the energy deposition duration t_{ign} is set proportional to the flame characteristic time $\tau_f = \delta_f^0 / S_L^0$ in the current analyses. In a similar manner to several previous works [11, 32–36] t_{ign} is considered equal to $0.2\tau_f$. The ignition kernel total energy is computed from the temperature T_{ign} which is set to the burnt gases equilibrium temperature to prevent temperature to evolve far from validity range of the chemical scheme.

In order to prevent strong aspiration effects that may rise from the sudden change in the sensible enthalpy at the end of the energy deposit, an additional ramping term $\mathcal{S}(x)$ is introduced in the source term given by the equation (13) such as:

$$\dot{Q}_{ign}(\mathbf{x},t) = \mathcal{S}\left(\frac{t}{t_{ign}}\right)\frac{(\rho h_s)_{ign}(\mathbf{x},t) - \rho h_s(\mathbf{x},t)}{t_{ign}}\exp\left(-\frac{r^2}{2R_{ign}}\right)\Big(H(t) - H(t_{ign})\Big), \tag{15}$$

with

$$\mathcal{S}(x) = \frac{1}{\alpha_{ign}^2}\begin{cases}\dfrac{1-x}{1-\alpha_{ign}} & \text{if } x \geq \alpha_{ign}\\ 1 & \text{otherwise,}\end{cases} \tag{16}$$

where α_{ign}^2 is a constant threshold considered to be in the order of 0.1.

D. DNS database parameters

The present DNS database features six configurations. These eight computations can be viewed as two groups of three calculations, where the first group refers to variable non-unity Lewis number (VL), whereas the second corresponds to constant unitary Lewis number (CL). In both categories, two draws of turbulent field and two draws of the initial equivalence ratio field were considered. The values of L_Φ are set proportional to the turbulent integral length scale l_t in such a way that the three stratified cases are characterized by smaller ($L_\Phi = l_t/2$), comparable ($L_\Phi \simeq l_t$) and larger ($L_\Phi = 2l_t$) fluctuations length-scale than the turbulent flow field. The operational conditions and the setup of the DNS database cases are summarized in Table 1. In the latter, l_t, τ_t and η refer to the turbulent integral length scale, eddy turnover time, and the Kolmogorov length scale,

respectively. u_{rms} denotes velocity fluctuations root mean square (rms). S_L^0, δ_f^0 and τ_f denote the laminar flame speed, the thermal flame thickness, and the chemical time scale, respectively. All the configurations are undertaken on a regular Cartesian grid of size $36\delta_L^0$, discretized on 512^3 cells, which ensures that about 15 grid points are within the flame thickness. Moreover, to ensure that the small scales are resolved in the considered case, the spatial discretization step Δx is adjusted such that $\eta/\Delta x \sim 1.5$.

Operating conditions			
P (atm)	$\overline{\Phi}$	T_u (K)	
1.0	0.8	500	
Chemistry			
δ_L^0 (mm)	S_L^0 (m/s)	τ_c (ms)	
0.23	0.85	0.45	
Turbulence			
l_t (mm)	η (mm)	u_{rms} (m/s)	τ_t (ms)
2.32	0.011	8.51	0.27
Dimensionless numbers			
Da	Ka	Re_t	
0.6	12.9	60.0	

Table 1 DNS simulations characteristics

III. Preliminary results and discussion

The temporal evolutions of the integral heat release rate evaluated as the volumetric integral of the local heat release $\dot{\omega}_{HRR}$, *i.e* , $\dot{\Omega}_{\mathrm{HRR}} = \int_V \omega_{\dot{\mathrm{HRR}}} \mathrm{d}V$ are reported in fig. 1 for constant and variable Lewis numbers for the three considered values of L_Φ.

Since the energy deposit duration is the same for all the case, we use it to normalize the time in fig. 1 and subsequent figures showing temporal evolutions. At the end of the duration of the forced energy deposit, the temperature of the kernel decreases due to the strong gradient between burnt and fresh gases. This drop in temperature leads to a decreasing of the heat release with the kernel growth. At this stage, the stratification length-scale does not seem to be of strong influence on the evolution of $\dot{\Omega}_{\mathrm{HRR}}$ for the (VL) cases. On the other hand, noticeable differences can be seen when fuel Lewis number is constant. Indeed, small scale stratifications lead to a larger global heat release during the times following the forced ignition. Independently

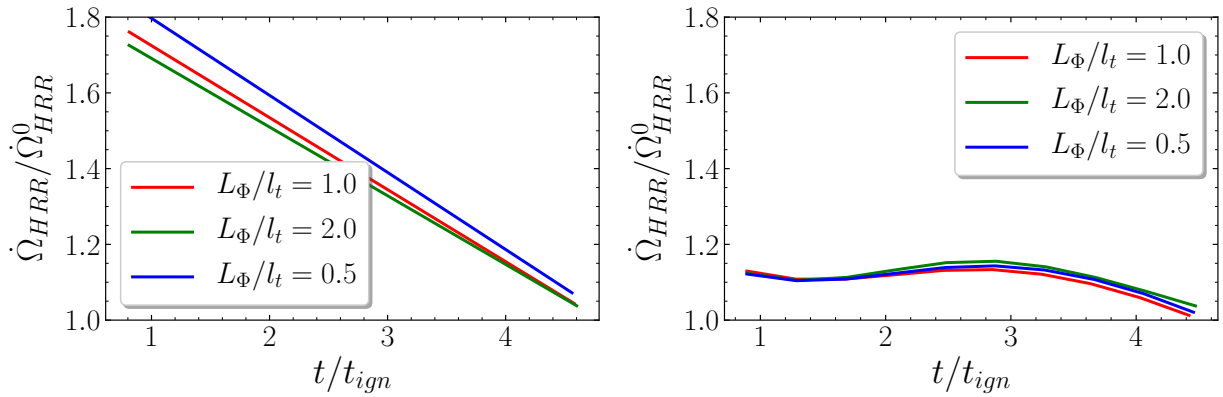

(a) Constant fuel lewis number **(b) Variable fuel Lewis number**

Fig. 1 Temporal evolution of the normalized volumetric integral heat release rate $\dot{\Omega}_{\mathrm{HRR}}$ for the three stratification length scales.

of the stratification scale, we notice that the burning extent, given here by $\dot{\Omega}_{\mathrm{HRR}}$, is more pronounced for the (CL) cases in comparison with the (VL) cases, which is consistent with the previous findings [9].

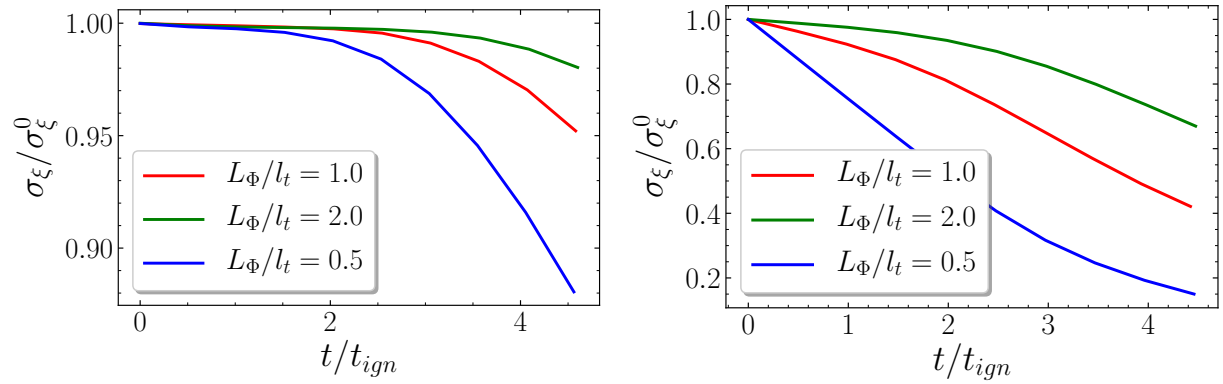

(a) Constant fuel lewis number **(b) Variable fuel Lewis number**

Fig. 2 Temporal evolution of the normalized standard deviation of the mixture fraction field on the flame front

A possible explanation for the results exposed above relies on the evolution of the mixture fraction distribution on the flame front. Indeed, molecular diffusion and mixing in fresh gases tend to homogenize the mixture. However, as the velocity fluctuations and the integral length scale are set initially equal for all cases, the flame kernel growth at this stage is mainly driven by the distribution of the fresh mixture. As stated in previous works [37], the turbulent mixing efficiency decreases with the characteristic length scale. This statement is supported by fig. 2, which reports the temporal evolution of the standard deviation σ_ξ of the

mixture fraction field on the flame front normalized by its value at the initial state. Here, The flame front is defined as the progress variable iso-surface $c = 0.7$, where c is the progress variable based on temperature

$$c(\mathbf{x}, t) = \frac{T(\mathbf{x}, t) - T_u}{T_b(\xi(\mathbf{x}, t)) - T_u},$$

with $T_b(\xi(\mathbf{x}, t))$ is the burnt gases temperature given for a mixture fraction. For both variable and constant fuel Lewis numbers, the standard deviation tends to decrease more quickly as the stratification field length scale increases. However, we notice that the evolution of the mixture fraction distribution toward a homogeneous state is slower in the (CL) cases. This can be attributed to the fact that in the case of variable fuel Lewis number, the flame front is subjected not only to turbulent mixing, but also to the molecular diffusion effects.

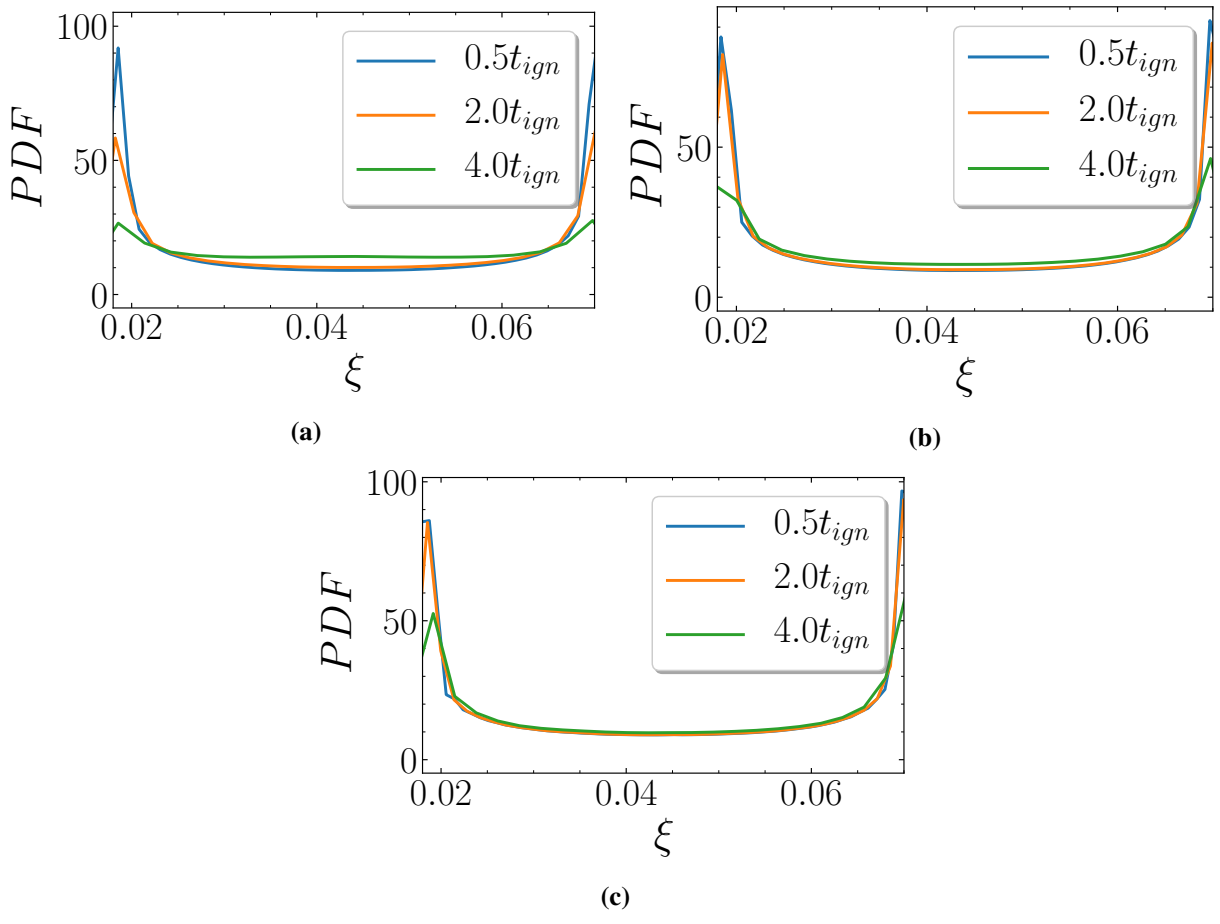

Fig. 3 PDF mixture fraction on the flame front at time $t = 4.5t_{ign}$ for constant lewis number cases. Left, $L_\Phi/l_t = 0.5$, middle $L_\Phi/l_t = 1.0$, right $L_\Phi/l_t = 2.0$

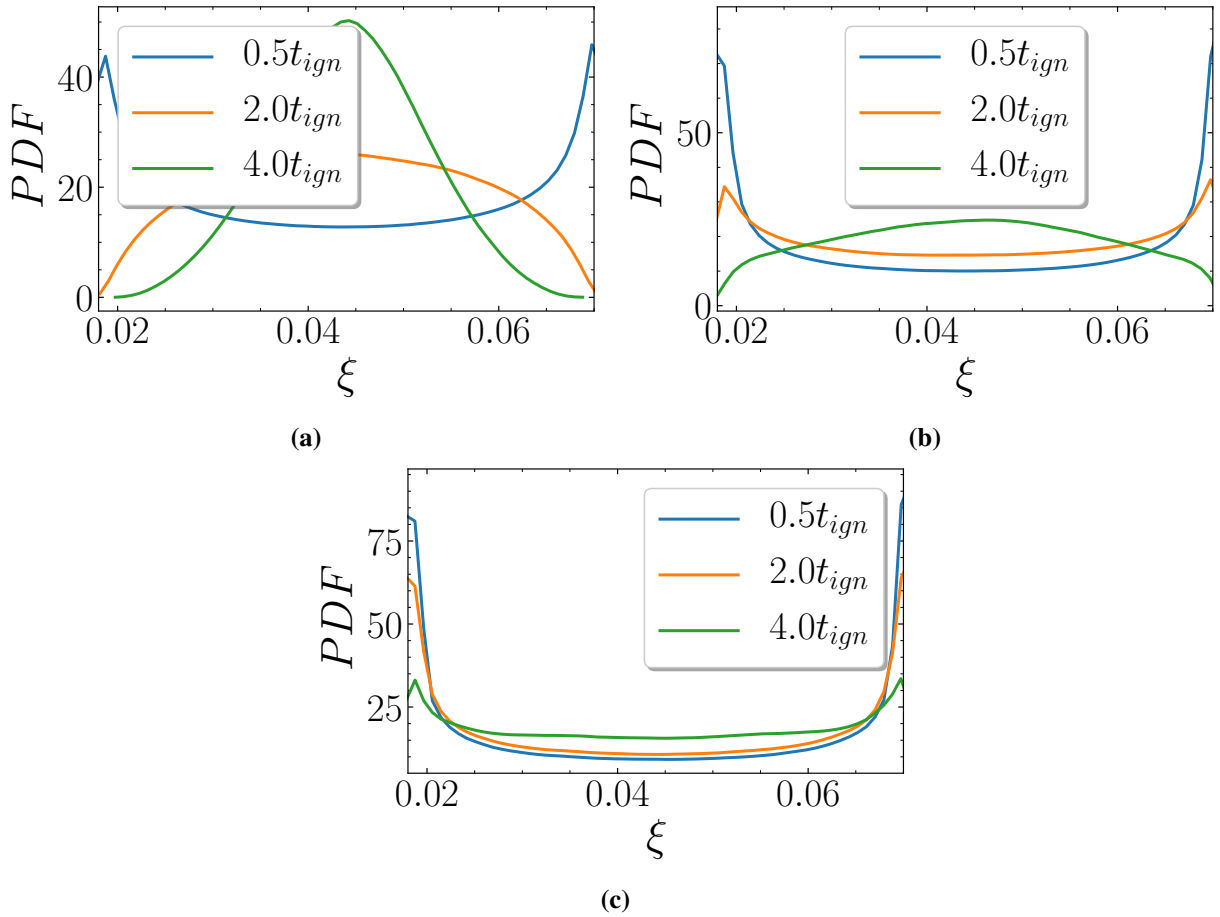

Fig. 4 PDF mixture fraction on the flame front at time $t = 4.5t_{ign}$ for variable lewis number cases. Left, $L_\Phi/l_t = 0.5$, middle $L_\Phi/l_t = 1.0$, right $L_\Phi/l_t = 2.0$

This trend is more visible on figures 3, 4 which present the PDFs of the mixture fraction on the flame front for (CL) and (VL) respectively. In the case of constant Lewis number the mixture fraction distribution preserves its bi-modality independently from the value of L_Φ. On the other hand, in the (VL) cases the mixing effects are more pronounced as the kernel grows. Besides, it can be seen that L_Φ strongly affects the distribution of mixture fraction.

IV. Conclusions and upcoming work

Three dimensional direct numerical simulation database is generated to assess the joint effects of differential diffusion and the stratification characteristic length-scale L_Φ on a methane-air flame kernel development. The database considers both variable and constant fuel Lewis number with three distinct values

for the characteristic length scale of the stratified equivalence ratio field. The preliminary study conducted above on several ignition duration time t_{ign}, has shown similar trends to previous works in terms of heat release, which is found to be larger when the Lewis number is considered unitary. Moreover, it has been demonstrated that starting from this *early* combustion stage, the mixture fraction field is not as sensitive to the stratification length-scale L_Φ.

Acknowledgments

The research work was sponsored by King Abdullah University of Science and Technology (KAUST) and made use of the computer clusters at KAUST Supercomputing Laboratory (KSL) and the Supercomputing Laboratory and the Extreme Computing Research Center. The authors also thank Dr. Bilel Hadri at KSL for his technical assistance.

References

[1] Keck, J. C., Heywood, J. B., and Noske, G., "Early flame development and burning rates in spark ignition engines and their cyclic variability," *SAE Transactions*, 1987, pp. 162–175.

[2] Zhao, F., Lai, M.-C., and Harrington, D. L., "Automotive spark–ignited direct–injection gasoline engines," *Progress in Energy and Combustion Science*, Vol. 25, No. 5, 1999, pp. 437–562.

[3] Chakraborty, N., Hesse, H., and Mastorakos, E., "Effects of fuel Lewis number on localised forced ignition of turbulent mixing layers," *Flow, turbulence and combustion*, Vol. 84, No. 1, 2010, p. 125.

[4] He, L., "Critical conditions for spherical flame initiation in mixtures with high Lewis numbers," *Combustion Theory and Modelling*, Vol. 4, No. 2, 2000, pp. 159–172.

[5] Aung, K. T., Hassan, M. I., Kwon, S., Tseng, L. K., Kwon, O. C., and Faeth, G. M., "Flame/stretch interactions in laminar and turbulent premixed flames," *Combustion science and technology*, Vol. 174, No. 1, 2002, pp. 61–99.

[6] Saha, A., Chaudhuri, S., and Law, C. K., "Flame surface statistics of constant-pressure turbulent expanding premixed flames," *Physics of Fluids*, Vol. 26, No. 4, 2014, p. 045109.

[7] Goulier, J., Comandini, A., Halter, F., and Chaumeix, N., "Experimental study on turbulent expanding flames of lean hydrogen/air mixtures," *Proceedings of the Combustion Institute*, Vol. 36, No. 2, 2017, pp. 2823–2832.

[8] Echekki, T., Poinsot, T. J., Baritaud, T. A., and Baum, M., "Modeling and simulation of turbulent flame kernel evolution," *Transport Phenomena in Combustion, SH Chan (Ed.)*, Vol. 2, 1995, pp. 951–962.

[9] Alqallaf, A., Klein, M., and Chakraborty, N., "Effects of Lewis number on the evolution of curvature in spherically expanding turbulent premixed flames," *Fluids*, Vol. 4, No. 1, 2019, p. 12.

[10] Savard, B., Lapointe, S., and Teodorczyk, A., "Numerical investigation of the effect of pressure on heat release rate in iso-octane premixed turbulent flames under conditions relevant to SI engines," *Proceedings of the Combustion Institute*, Vol. 36, No. 3, 2017, pp. 3543–3549.

[11] Patel, D., and Chakraborty, N., "Localised forced ignition of globally stoichiometric stratified mixtures: A numerical investigation," *Combustion*

Theory and Modelling, Vol. 18, No. 6, 2014, pp. 627–651.

[12] Paolucci, S., *Filtering of sound from the Navier-Stokes equations*, Sandia National Laboratories Livermore, CA, USA, 1982.

[13] Poinsot, T., and Veynante, D., *Theoretical and numerical combustion*, RT Edwards, Inc., 2005.

[14] Er-Raiy, A., "Étude des processus élementaires impliqués en combustion à volume constant," Ph.D. thesis, Chasseneuil-du-Poitou, École nationale supérieure de mécanique et d'aérotechnique, 2018.

[15] Hirschfelder, J. O., Curtiss, C. F., Bird, R. B., and Mayer, M. G., *Molecular theory of gases and liquids*, Vol. 26, Wiley New York, 1954.

[16] Wilke, C. R., "A viscosity equation for gas mixtures," *The Journal of Chemical Physics*, Vol. 18, No. 4, 1950, pp. 517–519.

[17] Mathur, S., Tondon, P. K., and Saxena, S. C., "Thermal conductivity of binary, ternary and quaternary mixtures of rare gases," *Molecular Physics*, Vol. 12, No. 6, 1967, pp. 569–579.

[18] Coffee, T. P., "Kinetic mechanisms for premixed, laminar, steady state methane/air flames," *Combustion and flame*, Vol. 55, No. 2, 1984, pp. 161–170.

[19] Gordon, S., and McBride, B. J., "Computer program for calculation of complex chemical equilibrium compositions, rocket performance, incident and reflected shocks, and Chapman-Jouguet detonations," Tech. Rep. SP-273, NASA Lewis Research Center, 1971.

[20] Kim, J., and Moin, P., "Application of a fractional-step method to incompressible Navier-Stokes equations," *Journal of Computational Physics*, Vol. 59, No. 2, 1985, pp. 308 – 323.

[21] Falgout, R. D., and Yang, U. M., "HYPRE: A library of high performance preconditioners," *International Conference on Computational Science*, 2002, pp. 632–641.

[22] Cohen, S. D., Hindmarsh, A. C., and Dubois, P. F., "CVODE, a stiff/nonstiff ODE solver in C," *Computers in Physics*, Vol. 10, No. 2, 1996, pp. 138–143.

[23] Rogallo, R. S., "Numerical experiments in homogeneous turbulence," Tech. rep., NASA Lewis Research Center, 1981.

[24] Passot, T., and Pouquet, A., "Numerical simulation of compressible homogeneous flows in the turbulent regime," *Journal of Fluid Mechanics*, Vol. 181, 1987, pp. 441–466.

[25] Réveillon, J., "Numerical procedures to generate and to visualize flow fields from analytical or experimental statistics: Turbulent velocity, fluctuating scalars, and variable density sprays," *Journal of Flow Visualization and Image Processing*, Vol. 12, No. 3, 2005.

[26] Ruetsch, G. R., and Maxey, M. R., "Small-scale features of vorticity and passive scalar fields in homogeneous isotropic turbulence," *Physics of Fluids A: Fluid Dynamics*, Vol. 3, No. 6, 1991, pp. 1587–1597.

[27] Grout, R. W., Swaminathan, N., and Cant, R. S., "Effects of compositional fluctuations on premixed flames," *Combustion Theory and Modelling*, Vol. 13, No. 5, 2009, pp. 823–852.

[28] Bassenne, M., Urzay, J., Park, G. I., and Moin, P., "Constant-energetics physical-space forcing methods for improved convergence to homogeneous-isotropic turbulence with application to particle-laden flows," *Physics of Fluids*, Vol. 28, No. 3, 2016, p. 035114.

[29] Carroll, P. L., Verma, S., and Blanquart, G., "A novel forcing technique to simulate turbulent mixing in a decaying scalar field," *Physics of Fluids*, Vol. 25, No. 9, 2013, p. 095102.

[30] Vázquez-Espı, C., and Linan, A., "Thermal-diffusive ignition and flame initiation by a local energy source," *Combust. Theory Modelling*, Vol. 6, 2002, pp. 297–315.

[31] Chakraborty, N., Hesse, H., and Mastorakos, E., "Effects of fuel Lewis number on localised forced ignition of turbulent mixing layers," *Flow, turbulence and combustion*, Vol. 84, No. 1, 2010, p. 125.

[32] Wandel, A. P., "Extinction predictors in turbulent sprays," *Proceedings of the Combustion Institute*, Vol. 34, No. 1, 2013, pp. 1625–1632.

[33] Wandel, A. P., "Influence of scalar dissipation on flame success in turbulent sprays with spark ignition," *Combustion and Flame*, Vol. 161,

No. 10, 2014, pp. 2579–2600.

[34] Schroll, P., Wandel, A. P., Cant, R. S., and Mastorakos, E., "Direct numerical simulations of autoignition in turbulent two-phase flows," *Proceedings of the Combustion Institute*, Vol. 32, No. 2, 2009, pp. 2275–2282.

[35] Neophytou, A., Mastorakos, E., and Cant, R., "DNS of spark ignition and edge flame propagation in turbulent droplet-laden mixing layers," *Combustion and flame*, Vol. 157, No. 6, 2010, pp. 1071–1086.

[36] Patel, D., and Chakraborty, N., "Effects of energy deposition characteristics on localised forced ignition of homogeneous mixtures," *International Journal of Spray and Combustion Dynamics*, Vol. 7, No. 2, 2015, pp. 151–174.

[37] Lipatnikov, A. N., "Stratified turbulent flames: Recent advances in understanding the influence of mixture inhomogeneities on premixed combustion and modeling challenges," *Progress in Energy and Combustion Science*, Vol. 62, 2017, pp. 87–132.